




Cite this: *RSC Adv.*, 2018, 8, 32111

Synthesis and photoluminescence characteristics of high color purity $\text{Ba}_3\text{Y}_4\text{O}_9:\text{Eu}^{3+}$ red-emitting phosphors with excellent thermal stability for warm W-LED application

Jia Liang, Liangling Sun, G. Annadurai, Balaji Devakumar, Shaoying Wang, Qi Sun, Jialei Qiao, Heng Guo, Bin Li and Xiaoyong Huang *

Single phase Eu^{3+} -activated $\text{Ba}_3\text{Y}_4\text{O}_9$ ($\text{Ba}_3(\text{Y}_{1-x}\text{Eu}_x)_4\text{O}_9$) red-emitting phosphors with different Eu^{3+} doping concentrations were synthesized by a high temperature solid-state reaction method. The phase purity, crystal structure, photoluminescence properties, internal quantum efficiency, decay lifetimes, and thermal stability were investigated. Upon excitation at 396 nm near-ultraviolet light and 469 nm blue light, the $\text{Ba}_3(\text{Y}_{1-x}\text{Eu}_x)_4\text{O}_9$ phosphors exhibited a strong red emission at 614 nm due to the $^5\text{D}_0 \rightarrow ^7\text{F}_2$ transition of Eu^{3+} ions. The optimal doping concentration of Eu^{3+} ions in $\text{Ba}_3(\text{Y}_{1-x}\text{Eu}_x)_4\text{O}_9$ was found to be $x = 0.25$. Furthermore, the critical distance was calculated to be 12.78 Å and the energy transfer mechanism for the concentration quenching effect was determined to be quadrupole–quadrupole interaction. In addition, the Commission Internationale de l'Eclairage (CIE) chromaticity coordinates of $\text{Ba}_3(\text{Y}_{0.75}\text{Eu}_{0.25})_4\text{O}_9$ phosphors were measured to be (0.6695, 0.3302) which located at the red region, and significantly, the high color purity was about 97.9%. The as-synthesized phosphors also possessed excellent thermal stability and the activation energy was determined to be 0.29 eV. Therefore, the investigated results indicated that the $\text{Ba}_3\text{Y}_4\text{O}_9:\text{Eu}^{3+}$ phosphor may be a suitable candidate as a red phosphor for white light-emitting diodes under effective excitation at near-ultraviolet and blue light.

Received 19th July 2018
 Accepted 11th September 2018

DOI: 10.1039/c8ra06129g

rsc.li/rsc-advances

1. Introduction

During the past decades, frequency conversion using luminescent materials, which can convert incident radiation into desired wavelengths, has been widely applied in various fields, such as lighting, displays, bioimaging, sensors, and solar cells.^{1–6} In recent years, white light-emitting diodes (W-LEDs) have gradually replaced traditional incandescent and fluorescent lamps owing to their obvious advantages, such as high efficiency, low energy cost, environmental friendliness, and long lifetime.^{7–15} They are widely applied in residential lighting, automotive lighting, displays, and so on.^{16,17} For indoor illumination, the typical commercial W-LED is a combination of a blue InGaN LED chip with a yellow-emitting $\text{Y}_3\text{Al}_5\text{O}_{12}:\text{Ce}^{3+}$ phosphor. But the deficiency in the red region brings about a low color rendering index (CRI) and high correlated color temperature (CCT).^{18,19} In order to overcome the above defects, alternative W-LEDs have been developed using tricolor (red, green, and blue) phosphors pumped by near-ultraviolet (near-UV) LED chips.^{20,21} However, the current red phosphors like sulfides and oxysulfides ($\text{SrY}_2\text{S}_4:\text{Eu}^{2+}$ (ref. 22) and $\text{Y}_2\text{O}_2\text{S}:\text{Eu}^{3+}$

(ref. 23)) have poor chemical stability and are moisture insensitive. Recently, Eu^{2+} -activated nitrides compounds ($\text{Ba}_2\text{Si}_3\text{N}_8:\text{Eu}^{2+}$ (ref. 24) and $\text{CaAlSiN}_3:\text{Eu}^{2+}$ (ref. 25)) have been synthesized as red-emitting phosphors to overcome the above mentioned problems,²⁶ but the rigorous synthesis conditions such as high pressure, certain atmosphere, and high temperature restrict the practical applications. Therefore, it is significant to search novel red phosphors with excellent chemical stability, high-efficiency, good color purity, and especially high absorption in near-UV or blue wavelength region for W-LED application.

Rare-earth ions activated inorganic materials have been investigated extensively on account of their narrow emission bands and excellent luminescent properties.²⁷ Among them, the trivalent europium (Eu^{3+}) ion is a significant activator. In many inorganic compounds, Eu^{3+} ion mainly shows an efficient bright red emission around 615 nm attributing to intra 4f forbidden $^5\text{D}_0 \rightarrow ^7\text{F}_2$ transition.^{28–30} Meanwhile, the oxide phosphors are more stable in comparison with sulfide phosphors. In the past few years, oxide based phosphors have been widely investigated as potential candidates for W-LEDs applications.³¹ Li *et al.* have studied the color-tunable $\text{Bi}^{3+}/\text{Eu}^{3+}$ co-doped $\text{Ba}_3\text{Y}_4\text{O}_9$ phosphors; however, to our best knowledge, the Eu^{3+} single-doped BYO phosphors have not been reported and they may have better luminescence properties for further

College of Physics and Optoelectronics, Taiyuan University of Technology, Taiyuan 030024, P. R. China. E-mail: huangxy04@126.com



research. In this paper, we reported $\text{Ba}_3\text{Y}_4\text{O}_9:\text{Eu}^{3+}$ (BYO:Eu³⁺) red-emitting phosphors with superior thermal stability, internal quantum efficiency (IQE), and high color purity, which satisfied the potential application in fabrication of W-LEDs based on the near-UV/blue LED chip.

2. Experimental

2.1 Sample synthesis

The $\text{Ba}_3(\text{Y}_{1-x}\text{Eu}_x)_4\text{O}_9$ (abbreviated as BYO: $x\text{Eu}^{3+}$; $x = 0.10, 0.15, 0.20, 0.25, 0.30, 0.35,$ and 0.40) phosphors with different Eu^{3+} concentrations were synthesized *via* a conventional solid-state reaction route in an air atmosphere. Starting materials of BaCO_3 (analytical reagent), Y_2O_3 (99.99%), and Eu_2O_3 (99.99%) were weighed according to stoichiometric ratio and then mixed thoroughly in an agate mortar. Subsequently, the obtained mixtures were transferred into the alumina crucibles and sintered at 1400°C for 5 h in a furnace. Finally, when the samples cooled down slowly to room temperature, the obtained products were ground again into powders for further characterizations.

2.2 Characterization

The X-ray diffraction (XRD) patterns of the as-prepared phosphors were recorded on Bruker D8 Advance diffractometer with $\text{Cu-K}\alpha$ radiation ($\lambda = 1.54056 \text{ \AA}$). The morphology was analyzed by using a field-emission scanning electron microscope (FE-SEM; TESCAN MAIA3). The photoluminescence (PL) and photoluminescence excitation (PLE) spectra were examined by the Edinburgh FS5 spectrometer equipped with a 150 W continuous-wave xenon lamp. The IQE, decay curves, and temperature-dependent emission spectra of the samples were also measured by using the Edinburgh FS5 spectrometer equipped with an integrating sphere coated with barium sulfate, a pulsed xenon lamp, and a temperature controller.

2.3 Fabrication of the W-LED device

The commercial blue phosphor $\text{BaMgAl}_{10}\text{O}_{17}:\text{Eu}^{2+}$ (BAM:Eu²⁺), commercial green phosphor $(\text{Ba,Sr})_2\text{SiO}_4:\text{Eu}^{2+}$ and our red phosphor BYO:0.25Eu³⁺ were mixed thoroughly with silicone firstly, and then the obtained phosphor-silicone mixtures were coated on the surface of a 395 nm LED chip to fabricate a W-LED device. The fabricated device was driven by 3 V voltage and 60 mA current and the photoelectric properties of the device were measured by using an integrating sphere spectroradiometer system (HAAS2000, Everfine).

3. Results and discussion

The XRD patterns of BYO: $x\text{Eu}^{3+}$ ($x = 0.10, 0.15, 0.20, 0.25, 0.30, 0.35,$ and 0.40) phosphors were displayed in Fig. 1. It can be observed that all of the diffraction peaks were well-matched with the standard PDF#89-5891 card of $\text{Ba}_3\text{Y}_4\text{O}_9$, and there was no other impurity phase. In addition, due to the similar ionic radii between Y^{3+} ($r = 0.900 \text{ \AA}$, CN = 6; CN is the coordination number) and Eu^{3+} ($r = 0.947 \text{ \AA}$, CN = 6) ions,³² there was no obvious shift in the diffraction peaks. The radius percentage difference

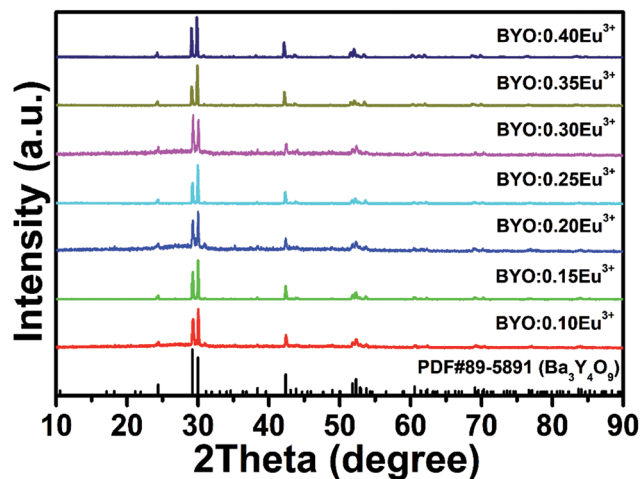


Fig. 1 XRD patterns of BYO: $x\text{Eu}^{3+}$ ($x = 0.10, 0.15, 0.20, 0.25, 0.30, 0.35,$ and 0.40) phosphors. The standard data of $\text{Ba}_3\text{Y}_4\text{O}_9$ (PDF#89-5891) was shown as reference.

between the dopants (Eu^{3+}) and substituted ions (Y^{3+}) can be calculated by the following equation:³³

$$D_r = \frac{R_s(\text{CN}) - R_d(\text{CN})}{R_s(\text{CN})} \times 100\% \quad (1)$$

where D_r is the radius percentage difference; R_s and R_d represent the ionic radii of host ion and doped ion. In this case, the value of D_r was determined to be 5.2%, which was far smaller than 30%. The result further manifested that the doped ions entered into the host lattice smoothly without any significant influence on the crystal structure.

Fig. 2(a) represents the Rietveld XRD refinement of Eu^{3+} -activated BYO phosphors and the refined crystallographic parameters were summarized in Table 1. As shown, the experimental and calculated spectra were accordant with each other, indicating that the BYO compound belonged to trigonal system with $R3$ space group. Meanwhile, the cell parameters were $a = b = 6.12099 \text{ \AA}$, $c = 25.2800(8) \text{ \AA}$, and $V = 820.258(35) \text{ \AA}^3$. Fig. 2(b) shows the crystal structure of BYO, it can be seen that there were four types of Y atom sites, named as Y_n ($n = 1, 2, 3, 4$). All of the Y atoms were surrounded by 6 oxygen atoms to form octahedrons. In addition, there were three types of Ba atom sites in this crystal structure, defined as Ba1, Ba2, and Ba3, which were coordinated with 6, 6, and 3 oxygen atoms, respectively.³⁴ Considering the same valence state, Eu^{3+} ions preferred to occupy Y^{3+} sites rather than Ba^{2+} sites, which were consistent with the previous results.

The representative FE-SEM image of BYO:0.25Eu³⁺ phosphors was shown in Fig. 3(a). The obtained compounds consisted of aggregated and irregular particles with the size of several micrometers. Moreover, as displayed in Fig. 3(b), elements of O, Y, Ba, and Eu were observed, and the elemental mapping results implied that the elements in BYO were evenly distributed over the whole particles.

Since the optimal doping concentration was 0.25 mol, the representative PLE and PL spectra of BYO:0.25Eu³⁺ phosphors were shown in Fig. 4. The PLE spectrum contained a broad band



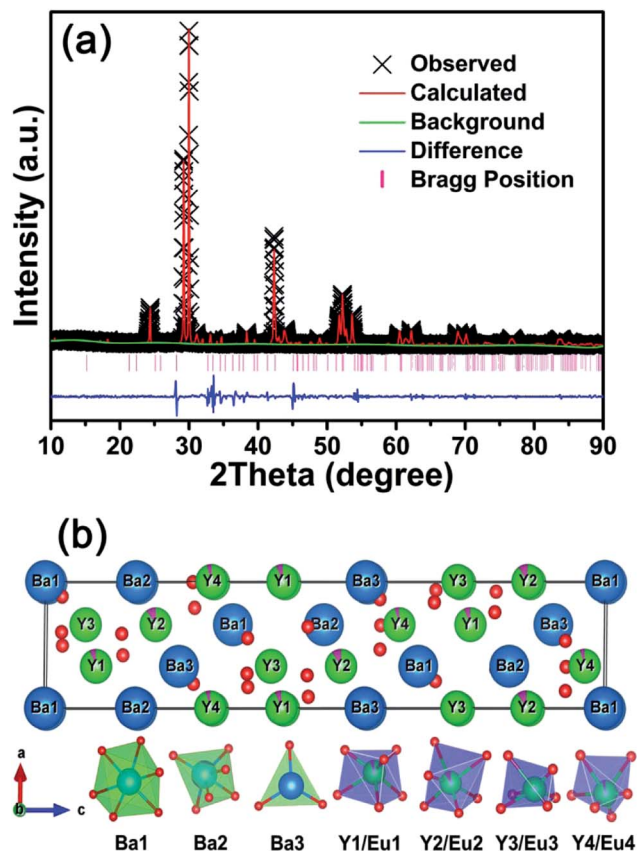


Fig. 2 (a) Rietveld refinement of BYO:0.25Eu³⁺ phosphors. (b) Crystal structure of BYO:0.25Eu³⁺ phosphors.

Table 1 Crystallographic and Rietveld refinement data of Ba₃Y₄-O₉:0.25Eu³⁺ phosphors

Formula	BYO:0.25Eu ³⁺
Space group	R3 - trigonal
<i>a</i>	6.12099 Å
<i>b</i>	6.12099 Å
<i>c</i>	25.2800(8) Å
α	90°
β	90°
γ	120°
<i>V</i>	820.258(35) Å ³

and several sharp peaks when monitored at 614 nm. The broad band ranging from 250 to 300 nm was attributed to O²⁻ → Eu³⁺ charge transfer band, which represented the electronic transition from 2p orbital of O²⁻ to empty 4f orbital of Eu³⁺. Meanwhile, several sharp excitation peaks located at 325, 366, 387, 396, 407, and 469 nm were assigned to ⁷F₀ → ⁵H₆, ⁷F₀ → ⁵D₄, ⁷F₀ → ⁵G₂, ⁷F₀ → ⁵L₆, ⁷F₀ → ⁵D₃, and ⁷F₀ → ⁵D₂ transitions, respectively.³⁵⁻³⁷ Particularly, the excitation intensities of ⁷F₀ → ⁵L₆ (396 nm) and ⁷F₀ → ⁵D₂ (469 nm) transitions were almost equivalent. Because the energy of near-UV light was larger than that of blue light, under the same situation, the PL intensity of BYO:0.25Eu³⁺ phosphors upon 396 nm excitation was stronger than that upon 469 nm, as shown in the PL spectra. The emission bands peaking at 594, 614, 656, and 704 nm were

ascribed to ⁵D₀ → ⁷F_{*J*} (*J* = 1, 2, 3, and 4) transitions of Eu³⁺ ions.³⁸⁻⁴⁰ Besides, the shape profiles of peaks had no variation except a slight change in PL intensity under the excitation of 396 and 469 nm, and also the strongest peak at 614 nm was ascribed to the ⁵D₀ → ⁷F₂ transition.

The magnetic dipole (MD) ⁵D₀ → ⁷F₁ transition (594 nm) is insensitive to the distortion of the inversion symmetry, and inversely the electric dipole (ED) ⁵D₀ → ⁷F₂ transition (614 nm) is hypersensitive.⁴¹ To evaluate the site symmetry of Eu³⁺ ions, the integrated PL intensity ratio (asymmetry ratio) (⁵D₀ → ⁷F₂)/(⁵D₀ → ⁷F₁) suggests the degree of distortion.⁴² In our case, the ED (614 nm) ⁵D₀ → ⁷F₂ transition was stronger than the MD (594 nm) ⁵D₀ → ⁷F₁ transition. The asymmetry ratio value of BYO:0.25Eu³⁺ was calculated to be 3.54, and others with different doping concentrations were listed in Table 2. This result revealed that the Eu³⁺ ions primarily occupied the non-inversion symmetry lattice sites in BYO host material.

Fig. 5(a) and (b) present the PL spectra of BYO:*x*Eu³⁺ phosphors with different doping concentrations under the excitation of 396 and 469 nm, respectively. It can be seen that the contours of the PL spectra hardly varied with the increase of the Eu³⁺ concentration. The normalized PL intensities of BYO:*x*Eu³⁺ phosphors as functions of Eu³⁺ concentrations under the excitation of 396 and 469 nm were displayed in Fig. 5(c). It was clearly found that the overall intensities under 469 nm excitation were slightly weaker than that under 396 nm excitation. These results indicated that the BYO:*x*Eu³⁺ phosphors can be effectively pumped with near-UV and blue LED chips. Moreover, the PL intensity gradually enhanced when Eu³⁺ ions concentration increased, then it reached a maximum at *x* = 0.25. Subsequently, when *x* was further increased, the PL intensity decreased due to the concentration quenching effect, which was triggered by the nonradiative energy transfer among the nearest Eu³⁺ ions.⁴³ According to the theory proposed by Blasse,⁴⁴ the concentration quenching mechanism can be determined by the critical distance (*R_c*) of Eu³⁺ ions. If *R_c* is larger than 5 Å, the electric multipolar interaction will lead to the concentration quenching phenomenon, otherwise it will be the exchange interaction. Therefore, it's necessary to calculate *R_c* via the following formula:⁴⁴

$$R_c = 2 \left(\frac{3V}{4\pi x_c N} \right)^{1/3} \quad (2)$$

where *V* is the volume of the unit cell, *x_c* is the critical concentration and *N* refers to the number of formula units per unit cell. In this present paper, *V* = 820.258 Å³, *N* = 3,⁴⁵ and *x_c* = 0.25. According to the above equation, the value of *R_c* was determined to be 12.78 Å and it was much larger than 5 Å. In BYO:*x*Eu³⁺ phosphors, the energy transfer among Eu³⁺ ions took place in the manner of electric multipolar interaction. In addition, to further research the interaction between Eu³⁺ ions in BYO:Eu³⁺ phosphors, Dexter's formula of multipolar interaction was used as expressed below:⁴⁶

$$I/x = K \left[1 + \beta(x)^{\theta} \right]^{-1} \quad (3)$$



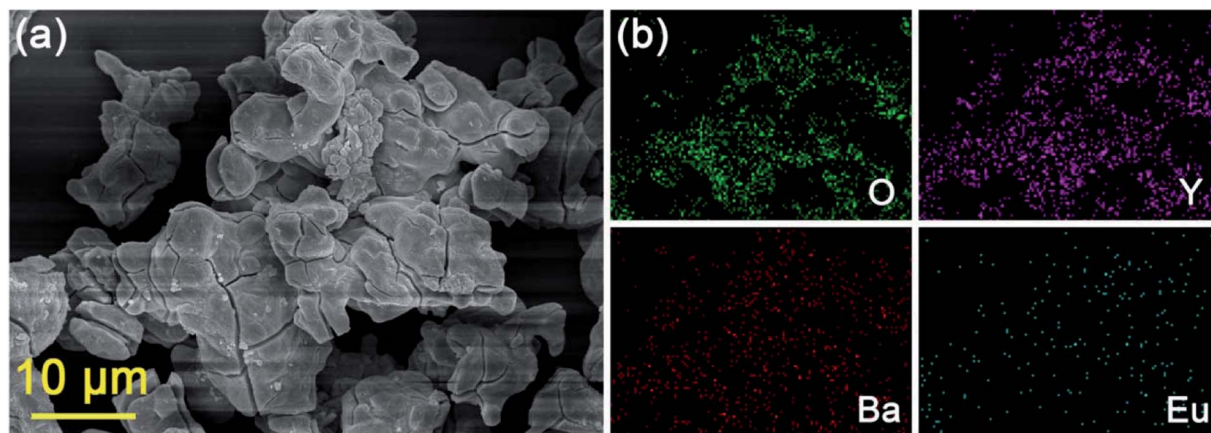


Fig. 3 (a) FE-SEM image of BYO:0.25Eu³⁺ phosphors. (b) Elemental mapping of BYO:0.25Eu³⁺ phosphors.

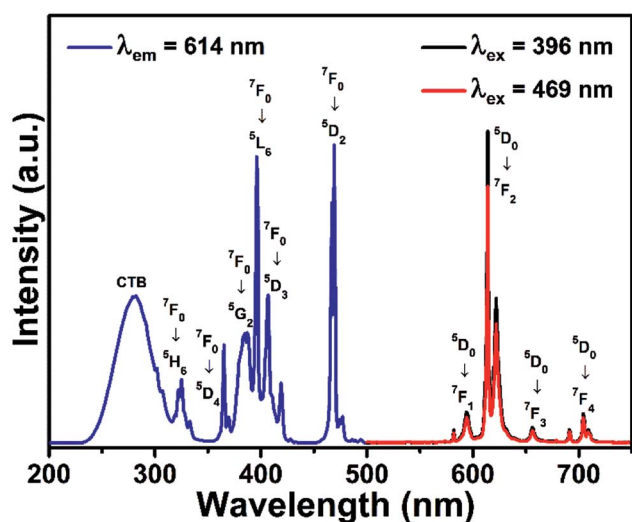


Fig. 4 PLE and PL spectra of BYO:0.25Eu³⁺ phosphors.

Table 2 The asymmetry ratio, CIE chromaticity coordinates, and color purity of BYO:Eu³⁺ phosphors with different Eu³⁺ concentrations

Eu ³⁺ concentration	Asymmetry ratio	CIE coordinates (x, y)	Color purity
0.10	3.36	(0.6662, 0.3335)	97.0%
0.15	3.50	(0.6682, 0.3316)	97.5%
0.20	3.48	(0.6689, 0.3308)	97.7%
0.25	3.54	(0.6695, 0.3302)	97.9%
0.30	3.41	(0.6685, 0.3312)	97.6%
0.35	3.40	(0.6678, 0.3320)	97.4%
0.40	3.24	(0.6662, 0.3335)	97.0%

where I is the emission intensity, x is the activator concentration, K and β are the constants for the same excitation condition, while $\theta = 6, 8,$ and 10 correspond to the dipole–dipole (d–d), dipole–quadrupole (d–q), and quadrupole–quadrupole (q–q) interactions, respectively. The slope of the fitting line between $\log(I/x)$ and $\log(x)$ was -3.7 , as shown in Fig. 5(d). Thus the value of θ was calculated to be 11.1 , which was close to 10 ,

indicating that the energy transfer among Eu³⁺ ions can be attributed to q–q interaction in BYO:Eu³⁺ phosphors.

The energy level diagram of Eu³⁺ ions was presented in Fig. 6(a) to demonstrate the energy transfer process. Upon the excitation of near-UV (396 nm) and blue (469 nm) light, the electrons at ground state (⁷F₀) transitioned to the higher excited states ⁵L₆ and ⁵D₂, then relaxed to lower excited state (⁵D₀) level through nonradiative transition. Subsequently, the lower excited state electrons returned to ⁷F_{*J*} ($J = 1, 2, 3,$ and 4) levels, resulting in four characteristic emissions due to the ⁵D₀ → ⁷F_{*J*} transitions, as shown in Fig. 6(a).

Fig. 6(b) shows the room-temperature decay curves of 614 nm red emission in BYO:*x*Eu³⁺ phosphors with different Eu³⁺ concentrations under the excitation of 396 nm. It's necessary to calculate the decay lifetimes and all the decay curves can be well fitted with the double-exponential equation:⁴⁷

$$I(t) = A_1 \exp(-t/\tau_1) + A_2 \exp(-t/\tau_2) \quad (4)$$

where $I(t)$ is the PL intensity at time t ; τ_1 and τ_2 represent the lifetimes for exponential components; A_1 and A_2 are constants. The average lifetime τ_s of Eu³⁺ can be calculated by the following function:⁴⁸

$$\tau_s = (A_1\tau_1^2 + A_2\tau_2^2)/(A_1\tau_1 + A_2\tau_2) \quad (5)$$

the τ_s were found to be 0.695, 0.650, 0.613, 0.521, 0.438, 0.231, and 0.187 ms for BYO:*x*Eu³⁺ phosphors with Eu³⁺ concentrations $x = 0.10, 0.15, 0.20, 0.25, 0.30, 0.35,$ and 0.40 , respectively. From Fig. 6(b), it was observed that τ_s dropped slowly at the beginning, when the Eu³⁺ concentration reached 0.25 mol, the decay lifetimes started to decline quickly, revealing the existence of the nonradiative energy transfer between the Eu³⁺ ions.

The CIE chromaticity coordinates are crucial factors to evaluate the luminescent properties of phosphors. Fig. 7(a) illustrates the CIE chromaticity diagram of BYO:0.25Eu³⁺ phosphors. According to the PL spectra, the CIE chromaticity coordinates of BYO:*x*Eu³⁺ phosphors ($\lambda_{\text{ex}} = 396$ nm) with various Eu³⁺ concentrations were summarized in Table 2. The green and blue asterisks in Fig. 7(a) represented the locations of CIE chromaticity



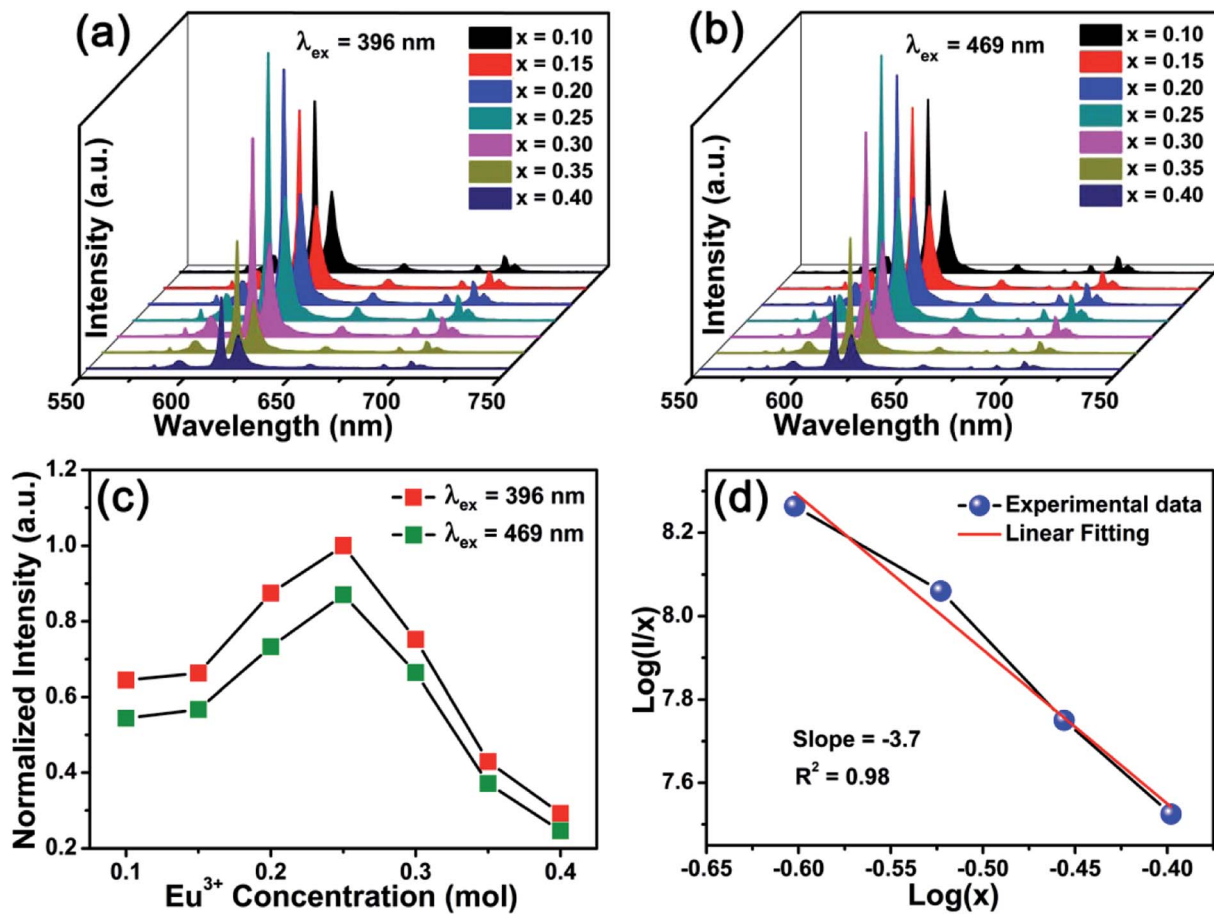


Fig. 5 (a) PL spectra of BYO: $x\text{Eu}^{3+}$ phosphors under 396 nm excitation. (b) PL spectra of BYO: $x\text{Eu}^{3+}$ phosphors under 469 nm excitation. (c) Normalized PL intensity of BYO: $x\text{Eu}^{3+}$ phosphors as a function of Eu^{3+} concentration. (d) Plot of $\log(I/x)$ vs. $\log(x)$ of Eu^{3+} ions in BYO: $x\text{Eu}^{3+}$ phosphors excited at 396 nm and monitored at 614 nm.

coordinates of BYO:0.25 Eu^{3+} phosphors under the excitation of 396 and 469 nm, respectively. The corresponding chromaticity coordinates were calculated to be (0.6695, 0.3302) and (0.6692, 0.3305), which were very close to that of the standard red light (0.6700, 0.3300).⁴² Furthermore, it can be clearly seen from

Fig. 7(a) that the both points basically coincided with each other, indicating that the phosphors can be excited efficiently by both near-UV and blue light from another point of view. The color purity was further investigated as follows:

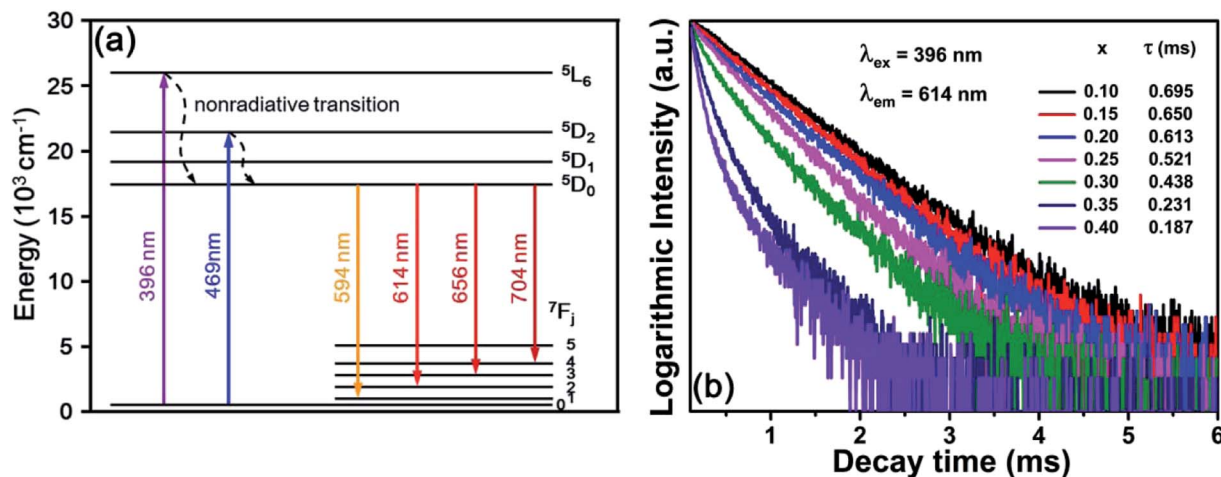


Fig. 6 (a) Energy level diagram of Eu^{3+} ions. (b) Decay curves of BYO: $x\text{Eu}^{3+}$ phosphors excited at 396 nm and monitored at 614 nm.



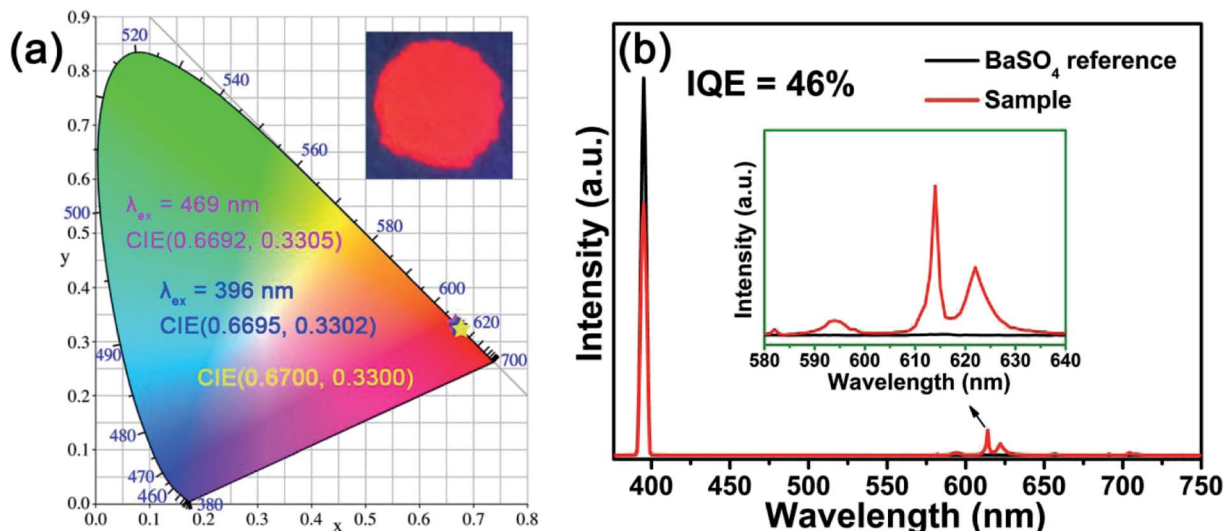


Fig. 7 (a) CIE chromaticity diagram of BYO:0.25Eu³⁺ phosphors under 396 and 469 nm excitation. Inset shows the photograph of BYO:0.25Eu³⁺ under a 365 nm UV lamp. (b) Excitation line of BaSO₄ and the emission spectrum of BYO:0.25Eu³⁺ phosphors collected using an integrating sphere. Inset shows a magnification of the emission spectrum in the 580–640 nm range.

$$\text{Color purity} = \frac{\sqrt{(x - x_i)^2 + (y - y_i)^2}}{\sqrt{(x_d - x_i)^2 + (y_d - y_i)^2}} \times 100\% \quad (6)$$

where (x, y) , (x_i, y_i) , and (x_d, y_d) present the CIE chromaticity coordinates of the sample, white illumination, and dominated wavelength, respectively. For BYO:0.25Eu³⁺ phosphors under 396 nm excitation, $(x, y) = (0.6695, 0.3302)$, $(x_i, y_i) = (0.310, 0.316)$, and $(x_d, y_d) = (0.6775, 0.3224)$. In this work, the value of color purity reached up to 97.9%, which was higher than that of Ca₂SiO₄:Eu³⁺ (91.2%),⁴⁹ NaBiF₄:Eu³⁺ (90.4%),⁵⁰ and CaWO₄:Eu³⁺ (91.3%),⁵¹ meaning that the high quality red-emitting BYO:0.25Eu³⁺ phosphors were obtained. The color purity of BYO:*x*Eu³⁺ samples with different Eu³⁺ doping concentrations were listed in Table 2.

Another key factor to assess the application of the phosphors is IQE. Fig. 7(b) depicts the IQE of the BYO:0.25Eu³⁺ red-emitting phosphors and the value of IQE can be obtained by the following equation:⁴⁵

$$\eta = \frac{\int L_S}{\int E_R - \int E_S} \quad (7)$$

where L_S is the emission spectrum of the sample, E_S and E_R are the spectra of excitation light with and without sample, respectively. Under 396 nm excitation, the IQE of BYO:0.25Eu³⁺ phosphor was calculated to be 46%, which was slightly higher than that upon 469 nm excitation (IQE: 40%). In addition, the external QE of BYO:0.25Eu³⁺ phosphors excited by near-UV light was found to be 5%.

Fig. 8(a) shows the temperature-dependent PL spectra of BYO:0.25Eu³⁺ phosphors excited at 396 nm. As the temperature increased from 303 K to 503 K, the PL intensity decreased gradually due to the thermal quenching effect. The normalized PL intensity of BYO:0.25Eu³⁺ phosphors as a function of temperature was depicted in the inset of Fig. 8(a). As shown, the

PL intensity at 423 K remained about 89% relative to its initial value at 303 K, which was higher than that of other reported Eu³⁺ doped phosphors, such as Ca₃Gd(AlO)₃(BO₃)₄:Eu³⁺ (84%)

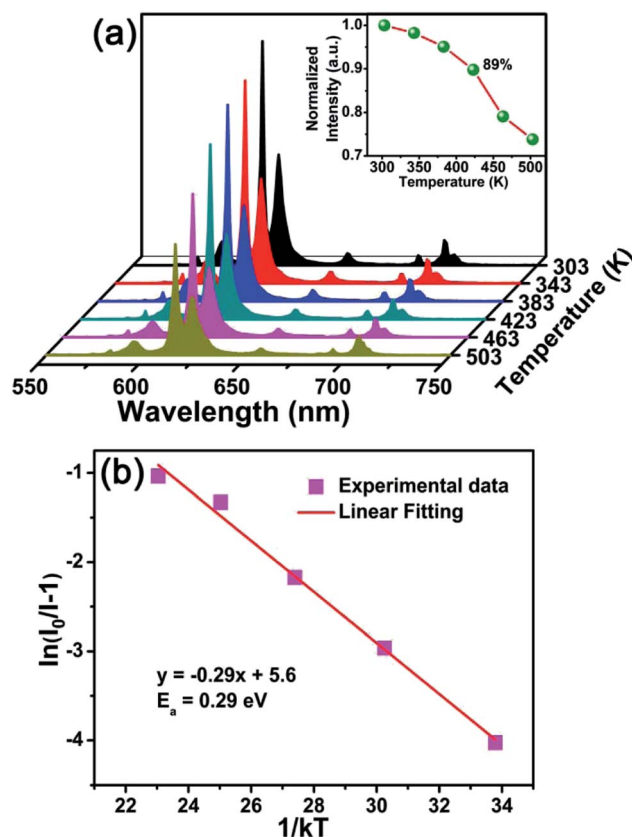


Fig. 8 (a) Temperature-dependent PL spectra of BYO:0.25Eu³⁺ phosphors excited at 396 nm. Inset shows the normalized PL intensity of BYO:0.25Eu³⁺ phosphors as a function of temperature. (b) Plot of $\ln(I_0/I - 1)$ vs. $1/kT$.



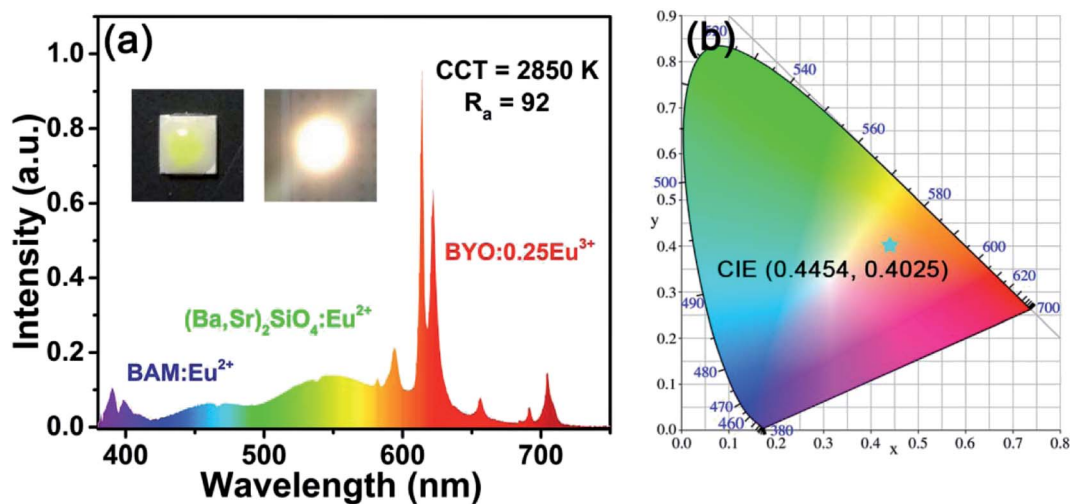


Fig. 9 (a) EL spectrum of the fabricated white LED device with 395 nm near-UV chip, BAM:Eu²⁺ blue phosphors, (Ba,Sr)₂SiO₄:Eu²⁺ green phosphors, and BYO:0.25Eu³⁺ red phosphors under 60 mA current. Inset shows the fabricated LED device and corresponding luminescent image. (b) CIE chromaticity diagram of the fabricated white LED device.

and Na₃Sc₂(PO₄)₃:Eu³⁺ (73.4%),^{33,52} indicating that the phosphors had a splendid thermal stability. Moreover, another parameter, activation energy was used to evaluate the thermal property according to the Arrhenius equation:⁵³

$$I(t) = \frac{I_0}{1 + c \exp(-E_a/kT)} \quad (8)$$

where I_0 is the PL intensity at room temperature, $I(t)$ is the PL intensity at different given temperatures, E_a is the activation energy, c is a constant, and k is the Boltzmann constant (8.629×10^{-5} eV). Fig. 8(b) illustrates the linear relationship between $\ln[(I_0/I) - 1]$ and $1/kT$, and the value of E_a was estimated to be 0.29 eV by the slope of the fitting line. Generally, the phosphors present superior thermal stability when E_a is high. The high E_a value suggested that the BYO: x Eu³⁺ phosphors possessed good thermal stability and were suitable for W-LEDs applications.

For further testing the application of BYO phosphors in W-LEDs, a W-LED device was fabricated based on 395 nm near-UV chip, commercial (Ba,Sr)₂SiO₄:Eu²⁺ green-emitting phosphors, commercial BAM:Eu²⁺ blue-emitting phosphors, and as-prepared BYO:0.25Eu³⁺ red-emitting phosphors. As disclosed in Fig. 9, under 60 mA current and 3 V voltage, the device gave bright warm white light with high CRI (92) and low CCT (2850 K). The CIE chromaticity coordinates of the W-LED device were (0.4454, 0.4025), which located at warm white range. The above results further demonstrated that the Eu³⁺-activated BYO phosphors had potential application for warm W-LEDs.

4. Conclusion

In summary, the BYO: x Eu³⁺ red phosphors were synthesized *via* a conventional solid-state reaction. The BYO: x Eu³⁺ phosphors which can be effectively excited at 396 nm (near-UV) and 469 nm (blue) exhibited an intense red emission around 614 nm. The optimal concentration of Eu³⁺ was $x = 0.25$. Furthermore, the CIE chromaticity coordinates of BYO:0.25Eu³⁺ phosphors were

(0.6695, 0.3302) and the value of IQE reached up to 46%. Meanwhile, the BYO:0.25Eu³⁺ phosphors also exhibited high thermal stability due to the fact that their PL intensity at 423 K maintained 89% of its starting value at 303 K and the activation energy was up to 0.29 eV. And in addition, a warm W-LED device with excellent properties was fabricated with the help of a 395 nm chip, as-prepared BYO:0.25Eu³⁺ red phosphors, commercial (Ba,Sr)₂SiO₄:Eu²⁺ green-emitting phosphors, and commercial BAM:Eu²⁺ blue-emitting phosphors. All of the obtained results suggested that our BYO: x Eu³⁺ phosphors were promising candidates for warm W-LEDs application pumped by both near-UV and blue light.

Conflicts of interest

There are no conflicts to declare.

Acknowledgements

This work was supported by the National Natural Science Foundation of China (No. 51502190), the Program for the Outstanding Innovative Teams of Higher Learning Institutions of Shanxi, and the Open Fund of the State Key Laboratory of Luminescent Materials and Devices (South China University of Technology, No. 2017-skllmd-01).

References

- 1 L. Xi, Y. Pan, S. Huang and G. Liu, *RSC Adv.*, 2016, **6**, 76251–76258.
- 2 M. Jiao, Q. Xu, C. Yang and H. You, *RSC Adv.*, 2017, **7**, 28647–28654.
- 3 Y. Hua, D. Zhang, H. Ma, D. Deng and S. Xu, *RSC Adv.*, 2016, **6**, 113249–113259.
- 4 V. Kumar, S. Som, S. Dutta, S. Das and H. C. Swart, *RSC Adv.*, 2016, **6**, 84914–84925.



- 5 X. Huang, J. Liang, B. Li, L. Sun and J. Lin, *Opt. Lett.*, 2018, **43**, 3305–3308.
- 6 L. Li, Y. Pan, Z. Chen, S. Huang and M. Wu, *RSC Adv.*, 2017, **7**, 14868–14875.
- 7 W. Ran, H. M. Noh, B. K. Moon, S. H. Park, J. H. Jeong, J. H. Kim, G. Liu and J. Shi, *J. Lumin.*, 2018, **197**, 270–276.
- 8 X. Huang, *Nat. Photonics*, 2014, **8**, 748–749.
- 9 B. Wang, H. Lin, J. Xu, H. Chen and Y. Wang, *ACS Appl. Mater. Interfaces*, 2014, **6**, 22905–22913.
- 10 W. Wang, Y. Jin, S. Yan, Y. Yang, Y. Liu and G. Xiang, *Ceram. Int.*, 2017, **43**, 16323–16330.
- 11 D. Chen, Y. Zhou and J. Zhong, *RSC Adv.*, 2016, **6**, 86285–86296.
- 12 J. Zhang, X. Zhang, J. Zhang, W. Ma, X. Ji, S. Liao, Z. Qiu, W. Zhou, L. Yu and S. Lian, *J. Mater. Chem. C*, 2017, **5**, 12069–12076.
- 13 J. Li, Q. Liang, J. Y. Hong, J. Yan, L. Dolgov, Y. Meng, Y. Xu, J. Shi and M. Wu, *ACS Appl. Mater. Interfaces*, 2018, **10**, 18066–18072.
- 14 J. Li, J. Yan, D. Wen, W. U. Khan, J. Shi, M. Wu, Q. Su and P. A. Tanner, *J. Mater. Chem. C*, 2016, **4**, 8611–8623.
- 15 Y. Guo, B. K. Moon, B. C. Choi, J. H. Jeong and J. H. Kim, *RSC Adv.*, 2017, **7**, 23083–23092.
- 16 Z. Cheng, J. Yu, Y. Zhang and N. Zou, *J. Lumin.*, 2017, **192**, 1004–1009.
- 17 K. Park, H. Kim and D. A. Hakeem, *Dyes Pigm.*, 2017, **136**, 70–77.
- 18 X. Ding, G. Zhu, W. Geng, Q. Wang and Y. Wang, *Inorg. Chem.*, 2016, **55**, 154–162.
- 19 Y. Feng, J. Huang, C. Li, G. Hu, J. Liu and X. Yu, *J. Alloys Compd.*, 2017, **706**, 478–484.
- 20 X. Fu, W. Lu, M. Jiao and H. You, *Inorg. Chem.*, 2016, **55**, 6107–6113.
- 21 Y. Li, Z. Zhao, Z. Song, R. Wan, J. Qiu, Z. Yang, Z. Yin, X. Liu, Q. Liu and Y. Zhou, *J. Am. Ceram. Soc.*, 2015, **98**, 2170–2176.
- 22 K. Tian, S. Lian, D. Yin, C. Li, A. Zhu and H. Zhang, *Rare Met.*, 2006, **30**, 639–644.
- 23 C. Guo, L. Luan, C. Chen, D. Huang and Q. Su, *Mater. Lett.*, 2008, **62**, 600–602.
- 24 S. A. Khan, N. Z. Khan, Z. Hao, W. W. Ji, H. Abadikhah, L. Hao, X. Xu and S. Agathopoulos, *J. Alloys Compd.*, 2018, **730**, 249–254.
- 25 K. Uheda, N. Hirotsaki, Y. Yamamoto, A. Naito, T. Nakajima and H. Yamamoto, *Electrochem. Solid-State Lett.*, 2006, **9**, H22–H25.
- 26 Y. Jin, Y. Fu, Y. Hu, L. Chen, H. Wu, G. Ju, M. He and T. Wang, *Powder Technol.*, 2016, **292**, 74–79.
- 27 F. B. Dejene, *J. Lumin.*, 2018, **199**, 433–441.
- 28 Y. Zhang, Y. Li and Y. Yin, *J. Alloys Compd.*, 2005, **400**, 222–226.
- 29 X. Huang, H. Guo and B. Li, *J. Alloys Compd.*, 2017, **720**, 29–38.
- 30 B. Li, X. Huang, H. Guo and Y. Zeng, *Dyes Pigm.*, 2018, **150**, 67–72.
- 31 X. Huang, B. Li and H. Guo, *J. Alloys Compd.*, 2017, **695**, 2773–2780.
- 32 Q. Zeng, H. Liang, M. Gong and Q. Su, *J. Electrochem. Soc.*, 2008, **155**, H730–H733.
- 33 H. Guo, X. Huang and Y. Zeng, *J. Alloys Compd.*, 2018, **741**, 300–306.
- 34 H. Wu, Z. Hao, L. Zhang, X. Zhang, Y. Xiao, G. Pan, H. Wu, Y. Luo, L. Zhang and J. Zhang, *J. Mater. Chem. C*, 2018, **6**, 3459–3467.
- 35 X. Zhang, M. Chen, J. Zhang, X. Qin and M. Gong, *Mater. Res. Bull.*, 2016, **73**, 219–225.
- 36 L. Li, W. Chang, W. Chen, Z. Feng, C. Zhao, P. Jiang, Y. Wang, X. Zhou and A. Suchocki, *Ceram. Int.*, 2017, **43**, 2720–2729.
- 37 Q. Liu, L. Wang, W. Huang, L. Zhang, M. Yu and Q. Zhang, *J. Alloys Compd.*, 2017, **717**, 156–163.
- 38 J. Hou, X. Yin, F. Huang and W. Jiang, *Mater. Res. Bull.*, 2012, **47**, 1295–1300.
- 39 Q. Liu, L. Wang, W. Huang, X. Li, M. Yu and Q. Zhang, *Ceram. Int.*, 2017, **43**, 16292–16299.
- 40 X. Lu, H. Liu, X. Yang, Y. Tian, X. Gao, L. Han and Q. Xu, *Ceram. Int.*, 2017, **43**, 11686–11691.
- 41 T.-C. Chien, C.-S. Hwang, Y.-T. Nien and M. Yoshimura, *Ceram. Int.*, 2017, **43**, 9437–9442.
- 42 A. K. Vishwakarma, K. Jha, M. Jayasimhadri, A. S. Rao, K. Jang, B. Sivaiah and D. Haranath, *J. Alloys Compd.*, 2015, **622**, 97–101.
- 43 Z. Zhou, J. Zheng, R. Shi, N. Zhang, J. Chen, R. Zhang, H. Suo, E. M. Goldys and C. Guo, *ACS Appl. Mater. Interfaces*, 2017, **9**, 6177–6185.
- 44 G. Blasse, *Phys. Lett. A*, 1968, **28**, 444–445.
- 45 K. Li, H. Z. Lian, M. M. Shang and J. Lin, *Dalton Trans.*, 2015, **44**, 20542–20550.
- 46 D. L. Dexter, *J. Chem. Phys.*, 1953, **21**, 836–850.
- 47 X. Wu, Y. Jiao, O. Hai, Q. Ren, F. Lin and H. Li, *J. Alloys Compd.*, 2018, **730**, 521–527.
- 48 A. Fu, L. Zhou, S. Wang and Y. Li, *Dyes Pigm.*, 2018, **148**, 9–15.
- 49 L. Lakshmi Devi and C. K. Jayasankar, *Ceram. Int.*, 2018, **44**, 14063–14069.
- 50 P. Du, X. Huang and J. S. Yu, *Chem. Eng. J.*, 2018, **337**, 91–100.
- 51 X. Huang, B. Li, H. Guo and D. Chen, *Dyes Pigm.*, 2017, **143**, 86–94.
- 52 B. Li, S. Wang, Q. Sun, C. Lu, H. Guo and X. Huang, *Dyes Pigm.*, 2018, **154**, 252–256.
- 53 S. A. Arrhenius, *Z. Phys. Chem.*, 1889, **4**, 96–116.

